ELSEVIER

Journal of Molecular Graphics and Modelling 21 (2002) 227–240

Journal of Molecular Graphics and Modelling

www.elsevier.com/locate/JMGM

Stochastic molecular dynamics of peanut lectin PNA complex with T-antigen disaccharide

Ernesto R. Caffarena [a], J. Raúl Grigera [b,*], Paulo M. Bisch [a]

[a] *Instituto de Biofísica, Carlos Chagas Filho, UFRJ, Rio de Janeiro, Brazil*
[b] *Instituto de Física de Líquidos y Sistemas Biológicos, (IFLY SIB) CONICET-UNLP-CIC, C.C. 565. Calle 59 No. 789, c.c. 565, 1900, La Plata, Argentina*

Abstract

The stochastic boundary molecular dynamics simulation method was applied to investigate the structure of a complex comprised of a tetrameric peanut lectin and the tumour-associated disaccharide, Galβ1-3GalNAc (T-antigen). Only a small region encompassing the active site was explicitly included in the calculations, but the electrical contribution of most outer atoms was taken into account by adding to the effective potential a term coming from an electrostatic potential grid that was pre-calculated and used to approximate the electrostatic energy and the force at any point in the interacting site. Results of simulating the intermolecular hydrogen bond network agree fairly well with X-ray experiments. An estimation of the direct and water-mediated interaction mean lifetimes and mean water residence times around the T-antigen oxygen atoms was computed over 400 ps. Monitoring the behaviour of water molecules within the active site revealed that there is a constant exchange of water with the bulk, especially in the proximity of ASN41, ASN127 and GLU129. The temporal evolution of the glycosidic linkage was also investigated and compared with simulations of T-antigen in solution. These studies of peanut lectins–sugar complexes clearly emphasize the importance of bound water molecules in generating carbohydrate specificity.

Keywords: Lectins; Stochastic molecular dynamics simulation; PNA; T-antigen

1. Introduction

Lectins mediate cell recognition in a wide range of biological systems and have attracted considerable attention in recent years, owing of their potential for use in the study of biological receptors and cell-surface phenomena. These proteins, for example, have proven to be highly useful models with which to study the molecular basis of protein carbohydrate recognition; their various carbohydrate specificities have made them important research tools in areas of glycobiology, immunology, parasitology and medicine. More specifically, lectins appear to serve mediators in the defence against invading organisms [1]. They also participate, among others things, in the symbiotic association between nitrogen fixing bacteria and the roots of leguminous plants [2,3], the recognition of host cells by viruses [2] and the adhesion of viruses, bacteria and protozoa to host cells and of leukocytes to endothelial cells [1].

Of particular interest are lectin–oligosaccharide complexes since they provide a basis for understanding how lectins recognise their natural ligands. High-resolution X-ray crystallography and NMR studies of lectins in complex with their ligands have made it possible to identify the protein and carbohydrate chemical groups that interact with each other and the specific interactions that these groups establish [4–14], thereby enabling elucidation of the features important to carbohydrate binding.

The most representative and largest family of simple lectins studied is found in legumes. This large group of homologous proteins, which are abundant in the seeds of most leguminous plants and which specifically recognise the structures of complex carbohydrates, differ in their carbohydrate specificities but resemble each other in their structural and physicochemical properties. Though their physiological functions are still unknown, proposed functions include storage and/or transport of carbohydrates within seeds, binding of nitrogen-fixing bacteria to root hairs, and inhibition of fungal growth and insect feeding [3].

Typically a legume lectin consists of two or four identical or nearly identical subunits (25–30 kDa), each with a single small carbohydrate active site having the same specificity. It also contains a tightly bound Ca^{2+} and one transition metal ion, usually Mn^{2+}, per subunit, which are required for carbohydrate binding. These particular atoms are situated

* Corresponding author. Tel.: +54-221-425-49-04; fax: +54-221-425-73-17.
E-mail address: grigera@iflysib.unlp.edu.ar (J. Raúl Grigera).

1093-3263/02/$ – see front matter © 2002 Elsevier Science Inc. All rights reserved.
PII: S1093-3263(02)00119-5

about 4.25 Å apart, in the proximity of the carbohydrate binding site, where they help to position the amino acids that form the contacts with the carbohydrate, but they do not bind it directly. Also note that four structural water molecules are conserved in all legume lectins and participate directly or indirectly in metal binding [15].

Peanut lectin (PNA) is a homotetrameric protein of 110 kDa, which has a high specificity for Thompsen–Friedenreich antigen (T-antigen) disaccharide (Galβ1–3GalNAc) [4,7]. The four subunits in the tetrameric complex have identical structures; the primary structure of each consists of 236 amino acids and has the typical legume lectin fold (CATH code 2.60.120.60). PNA lectin has an unusual open quaternary structure. Perhaps the most remarkable aspect of this is the tetramer's lack of symmetry; it is not glycosylated and is made up of two dimers. The structure of PNA lectin in complex with T-antigen can be obtained from the Protein Data Bank using 2TEP code [8,9]. The protein in association with T-antigen was crystallised at neutral pH in an orthorhombic form containing the tetramer in the asymmetric unit. The structure of the protein was solved using the multiple isomorphous replacement method and refined to an *R*-value of 0.251 with a resolution of 2.5 Å.

Peanut lectin is widely used as a tool for recognizing T-antigen on the surfaces of malignant cells. T-antigen is a small, well-defined tumour-associated antigen of non-oncocefal origin present in more than 85% of human carcinomas, including those of the colon, breast, bladder, buccal cavity and prostate, and in other poorly differentiated cells [10–12]. Earlier crystallographic studies [7,8] revealed hydration of the active site to be of particular interest, since water molecules within the site effectively mediate carbohydrate–protein interactions.

Molecular dynamics (MD) simulations would seem to be an appropriate methodology with which to investigate in more detail the main interactions between PNA lectin and the T-antigen disaccharide. However, simulations of large complex biological systems using periodic boundary conditions are computer and memory demanding due to the necessity of including a sufficient number of solvent water molecules to reproduce more realistic behaviour. Therefore, in cases where the region of interest is spatially localised, it is useful to focus on a relatively small part of the system that includes only the binding site. When applying this approach, consideration of the stochastic boundary conditions would appear be a suitable methodology. Using that approach, Naidoo and Brady [16] performed simulations of the lectin from erythrina corallodendron in complex with two disaccharides molecules, Manα(1–3)Man and Manβ(1–4)GlcNAc, studying in detail the glycosidic linkage. In addition, Bradbrook et al. [14,17] carried out MD simulations on the same lectin in complex with a different set of saccharides, (α-galactose and *N*-acetyl lactosamine) as well as with concanavalin-A glucoside and manoside complexes. In addition to structural studies, this has also work focused on the thermodynamics of the binding process. Along the same line, Åqvist and Mowbray used a new theoretical approach that makes use of free energy calculations to compute the absolute binding constants for β-D-glucose and methyl-β-D-galactoside to the periplasmic glucose/galactose receptor from salmonella typhimurium [18]. All of these simulations were carried out using spherical systems centred on the active site with restrained boundary forces.

In the present analysis, we focused on the interaction between the PNA lectin and the T-antigen disaccharide using stochastic MD. We followed the simulation methodology used by Brooks and Karplus [23], incorporating the B-spline interpolation method to compute the mean electrical field contribution. In this way, we were able to include the long-range contribution of atoms excluded from the simulation. To our knowledge, this is the first time this procedure has been used to study a complex biological system.

2. Methodology

2.1. Force field

Simulations were performed using the THOR package [19], which makes use of the GROMOS [20,21] force fields. The carbohydrate atomic partial charges were taken from GROMOS96 [21], while the SPC/E model [22] was used to represent the water. The intramolecular interactions between bonded atoms (protein–protein and sugar–sugar) were represented by bond and valence angles and by torsion angle harmonic potentials. The SHAKE procedure was used to keep bonds lengths fixed with a relative geometric tolerance of 10^{-4}. The interaction between non-bonded atoms (intra- and intermolecular) was represented by a 6–12 Lennard Jonnes potential, and the electrostatic interaction between atomic partial charges was taken into account by adding a coulombic term to the expression for the effective potential. No explicit bonding functions were used for hydrogen bonds, since they were well represented by combining coulomb and Van der Waals parameters. The non-bonded and long-range electrostatic interactions were truncated using a cut-off radius of 10.5 Å and a shifting function that goes smoothly to zero as atom pair distances approach the cut-off, thus avoiding discontinuity in the coulombic potential term.

2.2. Computational methodology

As mentioned above, in cases where the region of interest is spatially localised, it is useful to focus on a relatively small part of the system. In this work, we have considered only the active site of the lectin, the substrate (T-antigen) and the surrounding water molecules. Successful application of this methodology requires special boundary conditions to mimic the behaviour of the whole system [23]. The system was therefore partitioned into three regions centering on the binding site (Fig. 1). Atoms located in the innermost region, termed the reaction region, affect the processes occurring

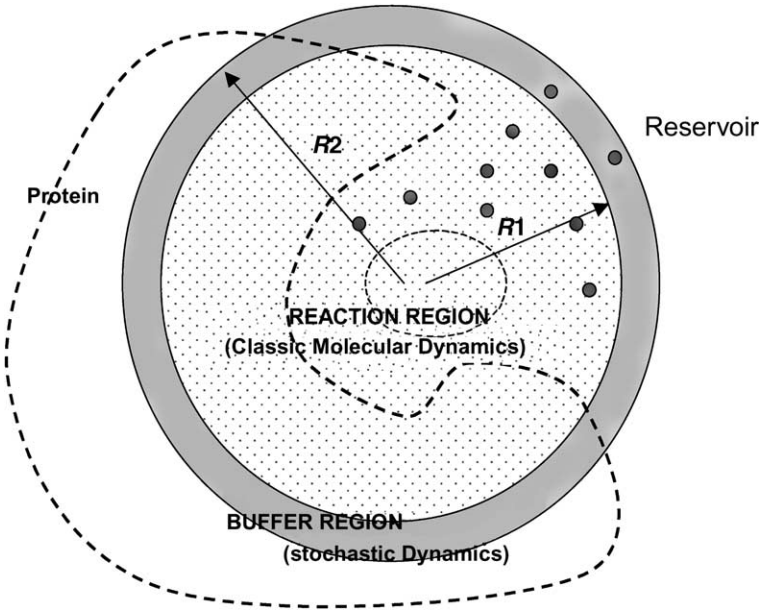

Fig. 1. Scheme of the partitioned system for stochastic dynamics. The irregular contour sketch the protein; R1, and R2 indicate the respective radius of the reaction region—all atom–atom interaction—and the region of the stochastic dynamics; the little circles represent the water. Water molecules that fare in the stochastic region are restrained to avoid loss of particles. The oval indicates the position of the ligand, which is taken as reference to select the center of the reaction region sphere.

at the active site. The full details of their dynamics are important, so they were simulated using standard MD. Atoms in the buffer region, the middle zone, evolve dynamically according to the Langevin equation; mean boundary and stochastic forces are applied in that region. Finally, the remainder of the system is called the reservoir region. The contribution of this region is evaluated indirectly, without explicitly considering the atoms present in the region.

The mean boundary forces contribute to the structural integrity and help to determine the fluctuations of reaction zone atoms, while stochastic forces provide a sink/source for thermal and spatial fluctuations occurring in the reaction zone. Boundary forces for the protein atoms are represented as linear restoring forces with the force constant derived from the atomic mean square fluctuations. Stochastic boundary forces mimic the energy flow between the reaction zone and reservoir region atoms. They also take into account the local fluctuations of the protein residues and the thermal exchange. Atoms that are not explicitly included in the calculation are in the reservoir region [23].

To compute the effect of the reservoir on the reaction region, a short full MD simulation of the entire system was carried out. This means that a complete simulation of the explicitly hydrated protein monomer and substrate molecules using periodic boundary conditions was performed in a classical way, solving Newton's laws of motion in the NPT ensemble.

The starting coordinates for the protein, sugar and crystallographic water molecules were obtained from the Brookhaven Protein Data Bank. The atoms of one molecule of the PNA tetramer (chain A in PDB file), the T-antigen in the binding site and 5889 water molecules, including the crystallographic ones, were put in a rectangular box with dimensions of 74 Å × 52 Å × 58 Å. By energy minimization, the system was relaxed to fit the crystallographic positions to the effective force field, after which 1000 steps of the steepest descent were carried out to optimize the molecular geometry. This procedure also diminished the effects of removing the other molecules in the tetramer and the rest of the crystallographic environment, which when compared to the crystal structure, resulted in a starting structure with a root mean square value of 0.18 Å. During the minimization the atoms of the protein and substrate were constrained to their positions with harmonic potential. The energy minimization was not exhaustive since it is applied only to relax the system enough to initiate the dynamics steps, which should reach the actual minimum.

The dynamical evolution of the system was computed by solving the equations of motion using the leap frog algorithm with constraints; time steps of 2 and 1 fs were used in the classical (full simulation) and stochastic procedures, respectively, thus ensuring a more stable convergence of the stochastic algorithm [24]. During the preliminary full simulation, the system was coupled to thermal and hydrostatic baths to maintain the room temperature (300 K) and atmospheric pressure (10,1325 Pa), respectively.

The whole system was heated from 10 to 300 K over the course of 10 ps, after which it was allowed to stabilise for 40 ps more. (Equilibration criteria was the fitting of the density trajectory to a straight line over the last 40 ps giving a value of 1.024 g/cm^3 with a slope of 10^{-5}.) Over the next 50 ps, trajectories were collected with which the parameters used in the stochastic dynamics were calculated. To prevent

the structure from shifting too far from the optimum, as the result of the new environment, we applied soft harmonic constraints ($k = 4.36\,\text{kcal mol}^{-1}\,\text{Å}^{-2}$ for backbone atoms, $k = 2.44\,\text{kcal mol}^{-1}\,\text{Å}^{-2}$ for side-chain atoms, and $10\,\text{kcal mol}^{-1}\,\text{Å}^{-2}$ for crystallographic water molecules) to all the protein atoms and to the crystallographic water molecules.

Simulations of T-antigen in solution were performed using periodic boundary conditions. T-antigen disaccharide was put in a cubic box, 25 Å on a side, with 468 SPC/E water molecules. After a 50 ps stabilisation period, the system evolved over 400 ps in the Gibbs Ensemble (NPT) using a time step of 2 fs.

When using the stochastic boundary conditions method, it was necessary to divide the protein, substrate and water molecules around the centre of the binding site and to calculate the appropriate mean and stochastic boundary forces. The initial position of the glycosidic oxygen atom of the T-antigen molecule was chosen to be the central point for partitioning the system and was held fixed during the simulations. The entire amino acid was considered in the volume if any atom of the backbone was less than 15.0 Å from the origin of the sphere. For the selected amino acids, if any atom of the side chain was less than 12.0 Å from the centre of the sphere the entire side chain was considered to be in the reaction region. We used a 15 Å radius for the reaction zone with a 3 Å wide buffer region. In all, there were 505 protein atoms, corresponding to 57 residues in the reaction zone, along with 280 water molecules. Metal atoms were considered explicitly in the sphere. Table 1 shows the residues included in the stochastic simulation. It also shows whether classical MD or stochastic dynamics affected the backbone and/or side-chain atoms.

For solvent atoms, the entire molecule was always included in one specific region, depending on the position of the oxygen atoms, and free water molecules could migrate between the simulated regions. To avoid diffusion of the free water molecules out of the sphere, a quartic potential function centred at the inner boundary of the buffer region was applied to them when they entered the buffer region [25]. In this region, we used a friction parameter, $\beta p = 250\,\text{ps}^{-1}$, for the protein atoms [23] and a friction coefficient, $62.36\,\text{ps}^{-1}$, which was calculated using the diffusion constant of the SPC/E model, for the water. Atoms belonging to the reservoir were excluded from dynamics simulations, though they were retained as a source of the mean electrostatic field calculated in the previous full simulation procedure. The B-spline method [26] was applied to the stochastic sphere to take into account long-range interactions of the reservoir atoms.

Before beginning the simulation, the electrostatic potential due to the reservoir atoms was computed for points lying on a three-dimensional grid that included the reaction zone. With the potential values previously calculated for the grid points using the standard B-spline interpolation method, a good approximation of the electrostatic potential could be obtained at any arbitrary point by interpolation. Van der Waals contributions were not considered because their range is short enough to be neglected.

A cube with a volume of $69\,\text{Å}^3$ was large enough to contain the sphere. Within it, there are 32,8509 points forming a grid, and for each point the electrostatic potential due to the excluded atoms was calculated. The 0.5 Å grid spacing used provided a good compromise between accuracy of the interpolation and storage requirements for systems of large size. The forces produced by the reservoir atoms on the atoms in

Table 1
List of residues included in the simulation

Amino acid	Region	Amino acid	Region	Amino acid	Region
ASP23	SD	GLY84	SD/CMD	SER126	CMD
THR35	SD	GLY99	SD	ASN127	CMD
ASN36	SD	SER100	SD/CMD	SER128	SD/CMD
LEU37	SD	ILE101	MD	GLU129	SD/CMD
ASN38	SD	GLY102	MD	TYR130	SD/CMD
LYS39	SD	GLY103	MD	ASN131	SD
VAL40	CMD	GLY104	MD	ASP132	SD/CMD
ASN41	CMD	THR105	SD/CMD	ASP136	SD
SER42	CMD	LEU106	SD/MD	VAL145	SD
VAL43	SD	GLY107	SD	ALA208	SD
GLY44	SD	VAL108	SD	SER209	CMD
ILE76	SD	SER109	SD	GLY210	CMD
LYS77	SD	ASP110	SD	SER211	CMD
ASP78	SD	THR111	SD/CMD	LEU212	CMD
TYR79	SD/CMD	LYS112	SD	GLY213	CMD
ASP80	CMD	GLY113	SD	GLY214	CMD
PRO81	CMD	ASP123	SD	ARG215	CMD
ALA82	CMD	THR124	SD/CMD	GLN216	SD/CMD
ASP83	CMD	TYR125	CMD	HIS218	SD

CMD: classical molecular dynamics; SD: stochastic dynamics.

the interior of the sphere were calculated by interpolating the previously calculated potential grid values, G_{ijk}, where i, j, and k are subscripts indicating the position of a point within the space of the grid. For the cubic spline, 64 points in a $4 \times 4 \times 4$ lattice were used to calculate the approximation of the potential at any point in the central cell of the lattice. The spline approximation was obtained by linear combination of the potential energy values (G_{ijk}) at the grid points comprising the 64 lattice points, each weighted by a product of the three cubic basis functions $B^3(x)$, $B^3(y)$, $B^3(z)$. The summation may be differentiated to provide the function gradient for force calculation.

$$\Phi(r) = \sum_{i=1}^{l+3} \sum_{j=1}^{m+3} \sum_{k=1}^{n+3} G_{ijk} B^3_{i-l}(r_x) B^3_{j-m}(r_y) B^3_{k-n}(r_z)$$

Fig. 2 illustrates the distribution of electrostatic potentials over the central orthogonal planes of the simulated region. In all the cases, the total contribution of the electrostatic field is almost negligible at the centre, but is relevant on the edges. This contribution to the effective force field also helps to maintain the molecular structure of the sphere region.

Once the spherical stochastic region was defined, a new system was heated, and stabilised well over 50 ps (equilibration criterion was the fitting to the density trajectory to a straight line over the last 40 ps with a slope les than 10^{-5} g cm^{-3}).

The trajectories were collected during 400 ps for later analysis. Simulations were carried out in a Pentium III (800 MHz) under LINUX Mandrake 7.0 operative system (kernel 2.2–7); partial analysis of the results and graphical display were carried out on a personal computer under Windows environment.

3. Results

3.1. Hydrogen bonds: comparison with crystallographic data

Crystallographic data indicate that both direct and water-mediated interactions are important for lectin binding to T-antigen disaccharide; Ravishankar et al. [8] found 10 direct hydrogen bonds and 5 water-mediated bridges. Our calculations show that a variety of other important hydrogen bonds, not observed by crystallography, are also established. We used a geometric criterion to characterise the formation of hydrogen bonds between the protein and the saccharide and between T-antigen and water molecules [27]. We proposed that a donor or an acceptor oxygen atom forms a hydrogen bond when the distance between the acceptor and the hydrogen atom was less than 2.4 Å and the H–O–H angle was between 145 and 215°. The hydrogen bond mean lifetimes were calculated as the rate of the total time for which the bond was found connected. If the hydrogen bond was found connected during two consecutive frames, we considered that it was not broken over the time elapsed. The duration of one connection is determined as the number of consecutive frames the hydrogen bond was found connected, times the simulation time step. Mean lifetimes of both direct and water-mediated interactions between T-antigen disaccharide and PNA lectin are shown in Table 2.

To analyse our results, we defined P as a measure of the persistence of the hydrogen bonds; as such P is the ratio (expressed as a percentage) of the time the hydrogen bond was found connected and the total simulation time. Our results show that some crystallographic hydrogen bonds appear with a very low P value. Hydrogen bonds with P values larger than 1% are listed in Table 2, though all crystallographic hydrogen bonds are listed regardless of their persistence. The mean distances of the hydrogen bonds during direct and water-mediated interactions are shown in Tables 3 and 4, respectively.

3.2. Direct interactions

All direct crystallographic hydrogen bonds with P values larger than 1% were reproduced in our simulations, with the exception of GLY104-N–GalO3, which has a negligible frequency and a very short mean lifetime (0.1 ps). This is most likely because the measured distance between GLY104-N and O3 was 3.2 Å [8], which is the limit for formation of a hydrogen bond. On the other hand, we observed an equivalent hydrogen bond formed between GLY104-N and the O2 oxygen of the galactose unit. This hydrogen bond was not observed in the crystallographic data, though in our calculations it had a P value of about 12%.

Comparing the calculated hydrogen bond distances with the crystallographic ones appearing in monomer one of the PDB file, we could see that the calculations placed the T-antigen closer to SER211, ASP80 and GLY213 and farther away from the ASN127 and ASP83 than the crystallographic data (Table 3). Although only the hydrogen bond between the OD2 oxygen atom of ASP80 and GalO6 was present in the crystallographic analysis [8], MD revealed that the interaction was not held solely by the OD2 oxygen atom, but also by the OD1 oxygen atom. That the former occurs more frequently may explain its appearance in the interpretation of the crystallographic data. If considered together, the two bonds sum to a P value of about 86%, making this the second strongest interaction obtained by analysis of MD results. The strongest interaction observed is the GLY213-N–GalNaCO4, which had a P value of 86% and a mean lifetime of 1.1 ps. The longest-lived hydrogen bond registered was the non-crystallographic one established between GalO4 and ASP80-OD1, which owing to the proximity of the groups involved lasted 6.6 ps. Other important non-crystallographic hydrogen bonds were also observed during the simulation process, including that formed between GalO4 and ASP80-OD1 (18%) and those between GalNAcO7 and GLY103 (33%), GLY104 (12%) and SER

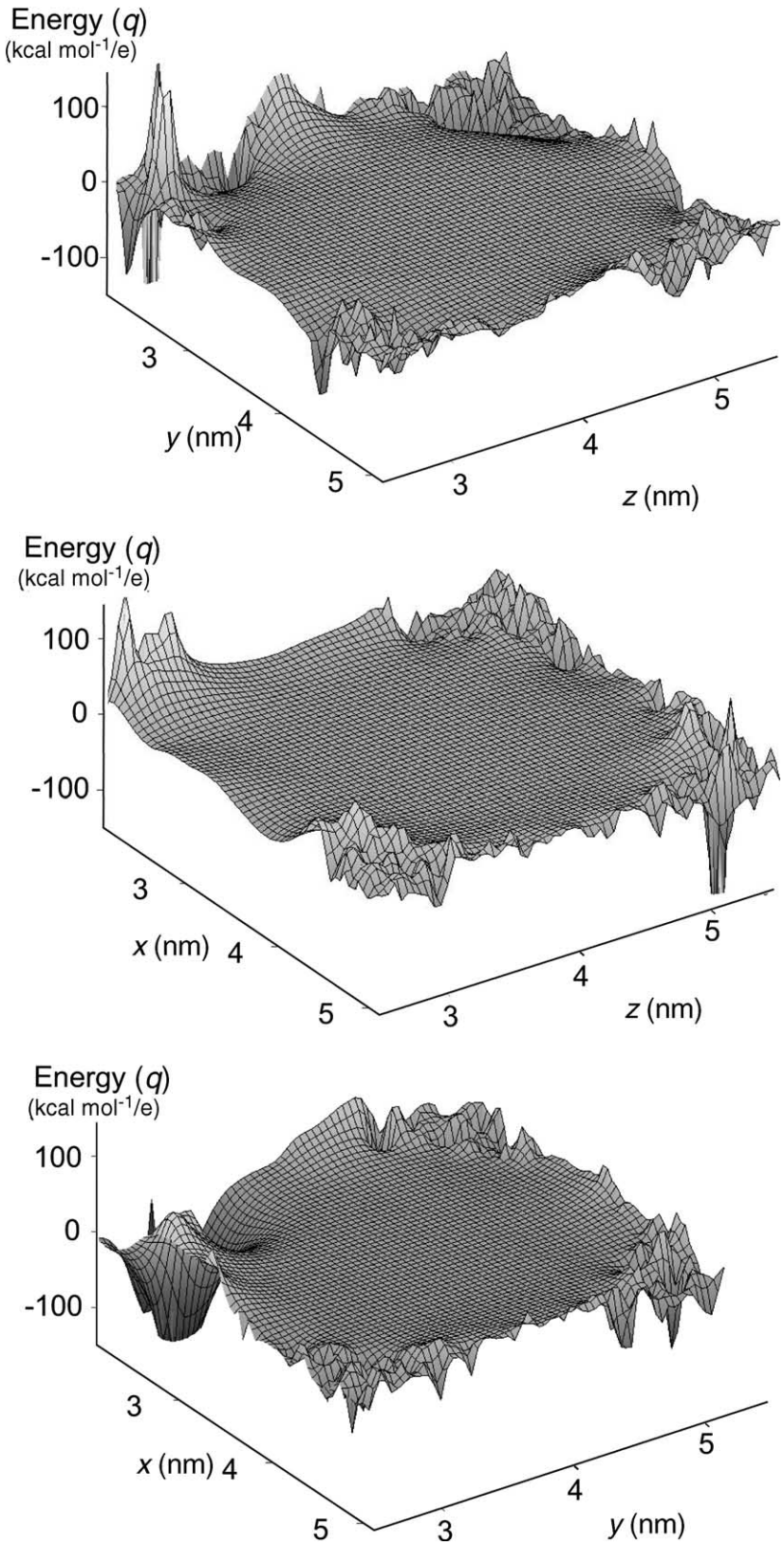

Fig. 2. Distribution of electrostatic potentials over the three central orthogonal planes of the simulation region. The electrostatic potential at every point of the grid represents the long-range contributions of atoms in the reservoir region, which was explicitly excluded from the simulations.

Table 2
Hydrogen bond interactions between T-antigen disaccharide and PNA lectin

Hydrogen bond	Mean lifetime (ps)	*P* (%)	Type
GalO1/GalNAcO3			
SER211-OG[a]	0.32	11	ACC
W–SER211-OG	0.27	4	AD
W–LEU212-N	0.15	3	AD
W–GalNAcO7	0.18	12	AA
GalO2			
W–GLY104-N[a]	0.39	25.5	AD
W–GLU129-OE2[a]	0.25	11	AA
W–GLU129-OE1[a]	0.58	60	AA
W–GLU129-OE2[a]	0.74	34	DA
W–GLU129-OE1[a]	0.22	2	DA
W–GalNAc-N2	0.32	1	DD
GalO3			
ASP83-OD1[a]	0.21	0	DON
GLY104-N[a]	0.12	0	DON
GLY103-N	0.40	6	DON
ASN127-ND2-HD1[a]	0.23	2	ACC
ASN127-ND2-HD2[a]	0.25	6	ACC
W–ASN127-ND2	0.84	43	DD
W–SER128-N	0.29	11	DD
W–ASP83-OD2	0.52	5	AA
W–GLU129-OE1	0.71	52	DA
W–GLU129-OE2	0.22	17	DA
W–THR124-O	0.15	1	AA
W–SER126-O	0.31	4	DA
GalO4			
ASP83-OD1[a]	0.70	2	DON
GLY103-N	0.18	14	DON
SER211-OG[a]	0.53	1	DON
SER211-OG[a]	0.86	40	ACC
GalO5			
SER211-OG[a]	0.28	13	ACC
W–GLY213-N	0.21	11	AD
W–GalNAcO4	0.21	11	AA
GalO6			
ASP80-OD1[a]	5.43	72	DON
GLY214-N	0.17	8	ACC
W–GLY213-N	0.26	22	AD
W–SER211-OG	0.34	3	AD
W–SER211-OG	0.36	1	AA
W–ASP80-OD1	1.61	21	DA
W–ASP80-OD2	0.39	2	DA
W–GalNAcO4	0.27	18	AA
W–GalNAcO6	0.40	21	AD
W–GalNAcO6	0.81	25	AA
GalNAcO1			
W–ILE101-O	0.16	1	DA
W–GalNAcO7	0.21	8	DA
W–GalNAcO7	0.31	6	AA
GalNAcN2			
W–GLU129-OE2	1.36	39	DA
GalNAcO4			
SER211-OG[a]	0.12	0	ACC
LEU212-N	0.18	2	ACC
GLY213-N[a]	0.49	5	ACC
W–GLY103-N	0.15	9.5	AD
W–ASN41-ND2	0.31	10	DD
W–LEU212-N	0.15	6	AD
W–LEU212-N	0.28	1	DD
W–GLY213-N	1.44	53	AD
W–SER211-OG	0.25	8	AD
W–ILE101-O	0.13	1	AA
W–ASN41-OD1	0.14	3	AA
W–SER211-OG	0.12	2	AA
W–GalNAcO7	0.18	11	AA
GalNAcO5			
GalNAcO6			
GLY213-N	0.13	1	ACC
W–GLY213-N	0.29	5	DD
GalNAcO7			
W–LEU212-N[a]	0.23	2	AD
W–ASN41-ND2[a]	0.33	11	AD
W–GLY103-N	0.19	16	AD
W–ILE101-O[a]	0.48	12	AA
W–SER211-OG	0.32	2	AD
W–SER211-OG	0.24	1.5	AA
W–TYR130-OH	0.40	4	AA

P is expressed in percentage and represents the persistence of the hydrogen bond during the simulation time. Column 'type' indicates the donor (DON) or acceptor (ACC) character: acceptor–acceptor (AA), donor–acceptor (DA), acceptor–donor (AD) and donor–donor (DD) in case of water-mediated interactions. The first letter makes reference to the carbohydrate molecule first group.

[a] Crystallographic hydrogen bonds

211 (12%). *P* values for these hydrogen bonds were not as high as the crystallographic ones, but values greater 30% suggest structural relevance.

3.3. Water-mediated interactions

A well hydrated active site and the existence of water-mediated hydrogen bonds are important to the specificity of the interactions between T-antigen the PNA lectin. Our simulation data revealed 23 water-mediated interactions, including those that appear in the crystallographic data. Although only one water bridge was observed between GLU129-OD1 and GalO2 in the crystallography, MD revealed that the OD2 oxygen atom also participated in the formation of a water bridge with almost the same persistence ($P \cong 19\%$) and comparable mean lifetimes. By analyzing the characteristics of the water bridges, we determined that the more probable state is obtained when GalO2 and the water molecule act as donor groups. This particular situation allows the water molecule to rotate and establish water bridges with the OD1 and OD2 oxygen atoms. We believe that formation of water bridges with both oxygen atoms of the GLU129 is most likely due to the mobility of the water molecule, rather than to the rotation of the acidic group. Nevertheless, while the situation in which GalO2 acts as an acceptor group occurs less frequently, it is not negligible.

Analyzing the GalO2–W–GLY104-N water bridge, it was observed that the water molecule was closer to the T-antigen

Table 3
Distances (Å) of PNA–T-antigen direct interactions

Hydrogen bond	Distance (Å)	Crystallographic distances (Å, unit 1)
GalO1/GalNAcO3–SER211-OG[a]	2.84 ± 0.16	3.15
GalO2–GLY104-N	2.97 ± 0.15	
GalO3–ASP83-OD1[a]	2.87 ± 0.14	2.71
GalO3–GLY104-N[a]	3.23 ± 0.05	3.22
GalO3–GLY103-O	2.95 ± 0.19	
GalO3–ASN127-ND2-H1[a]	3.06 ± 0.16	2.76
GalO3–ASN127-ND2-H2[a]	2.92 ± 0.17	2.76
GalO4–ASP80-OD1	2.82 ± 0.15	
GalO4–ASP83-OD1[a]	2.90 ± 0.18	2.71
GalO4–SER211-Og[a]	2.87 ± 0.19	2.97
GalO5–SER211-Og[a]	2.92 ± 0.16	3.02
GalO6–ASP80-OD1	2.80 ± 0.14	2.83
GalO6–ASP80-OD2[a]	2.80 ± 0.15	2.83
GalNAcO4–SER211-Og[a]	2.96 ± 0.16	3.33
GalNAcO4–LEU212-N	3.02 ± 0.13	
GalNAcO4–GLY213-N[a]	2.94 ± 0.16	3.29
GalNAcO7–ASN41-ND2	2.85 ± 0.16	
GalNAcO7–GLY103-N	2.87 ± 0.16	
GalNAcO7–GLY104-N	3.11 ± 0.15	
GalNAcO7–SER211-OG	2.65 ± 0.13	

Experimental values correspond to monomer one.
[a] Crystallographic hydrogen bonds.

than to the protein, which is consistent with the crystallographic findings. The other three crystallographic water bridges were established with the O7 of the GalNAc unit. Again, the water molecules are closer to the disaccharide than to the protein, with the most populated one being the non-crystallographic bridge GalNAcO7–W–SER211-OG (P = 31%; mean lifetime = 2.5 ps). Although analysis of the crystallographic data did not reveal the formation of this water bridge, by identifying the water molecules involved in the interaction, we were able to corroborate that this is the same water molecule that establishes the GalNAcO7–ASN41 (P = 3%) and GalNAcO7–LEU212 (P = 12%) water bridges. GalNAcO7 also makes a less probable and shorter contact with GLY103-N. In addition, GalO2 established a water bridge with ASN127 that had a short lifetime (0.3 ps) but had a considerable persistence (P = 11%), and GalO3 established a bridge with GLU129-OE1 (P = 19.5%; mean lifetime = 0.7 ps).

Saccharide molecules are hydroxylated compounds capable of establishing intramolecular, water-mediated interactions between their OH groups. These interactions were not discussed in the crystallographic works but probably have a role in the complex. Water-mediated interactions between saccharide groups in solution and in complex are shown in Table 5. A snapshot of a region of the active site en the environment of the T-antigen is shown in Fig. 3.

Most intramolecular, water-mediated interactions involving the T-antigen galactose unit were diminished or even lost when T-antigen complexed with PNA lectin. The water-mediated bridge between GalO2 and the nitrogen atom of the acetyl group shifted from P = 9% in the solution to P = 6% in the site. What is more, the GalO1/GalNAcO3–W–GalNAcO7, GalO3–W–GalO4, GalO4–W–GalO6, GalO5–W–GalNAcO4, GalO5–W–GalNAcO7 and GalO6–W–GalNAcO4 interactions vanished completely when the antigen complexed with PNA lectin.

By contrast, we observed one water bridge with a long mean lifetime that was established within the complex between GalO6 and GalNAcO6. This very stable water bridge, which occurred very frequently ($P \cong$ 30%) during the simulation time, could have a role in maintaining the stretched conformation of the sugar molecule. It is striking that this water bridge only appears within the complex and is not observed in the free sugar. In addition, the intramolecular GalNAcO1–W–GalNAcO7 and GalNAcO4–W–GalNAcO7 water bridges persisted when T-antigen was in the active site; indeed in both cases the relative frequency of persistence was increased within the complex.

3.4. Residence mean times

We computed the residence times of water molecules around the hydrophilic atoms of the T-antigen. Using a typical donor–acceptor hydrogen bond distance (radius = 3.5 Å), we computed the mean time that a water molecule remains within a sphere of that radius, regardless the formation of a hydrogen bond, and compared saccharide in solution with that in complex (Table 6).

Mean residence times for the atoms involved in the formation of water bridges (GalO2, GalNAcO1, GalNAcN2, GalNAcO6 and GalNAcO7) were longer when T-antigen was in complex than when it was in solution. It is worth noting that with the exception of the O4 oxygen atom in both units, in the water environment, all mean times were shorter than 1 ps. By contrast, when the saccharide was in complex, mean residence times were as long as 3 ps.

In Table 6, Q denotes the ratio (expressed as a percentage) of the time that at least one water molecule was found within the sphere (radius 3.5 Å) centered on a particular atom of the T-antigen and the total simulation time. In solution it is clear that most of the time, all of the OH groups of the sugar molecule had at least one water molecule within the sphere. In complex, however, no water molecules were found near GalO4, GalO5 or GalNAcO3 groups more than 70% of the time. On the other hand, the GalO2, GalO3, GalO6, GalNAcO1, GalNAcO6 and GalNAcO7 groups, which are involved in the formation of water bridges, yield Q values larger than 75%. Interestingly, the short mean residence lifetimes of these water molecules suggest they are constantly being replaced.

The existence of several water bridges involving various groups on the protein, T-antigen, and water molecules with mean residence times of less than 3 ps suggests that the same water molecules do not stay in the site for

Table 4
Distances of PNA–T-antigen water-mediated interactions

Hydrogen bond	Distance (Å)	Experimental distance (Å)	Distance (Å)	Experimental distance (Å)	Type
GalO2–W–GLY104-N[a]	OH–W = 2.83 ± 0.14	2.95	W–N = 2.93 ± 0.17	2.97	AD
GalO2–W–ASN127-ND2	OH–W = 2.82 ± 0.17		W–ND2 = 2.97 ± 0.15		DD
GalO2–W–GLU129-OE1[a]	OH–W = 2.81 ± 0.17	2.94	W–OE1 = 2.90 ± 0.15	3.36	DA
GalO2–W–GLU129-OE1[a]	OH–W = 3.04 ± 0.19		W–OE1 = 2.90 ± 0.15		AA
GalO2–W–GLU129-OE2	OH–W = 2.71 ± 0.14		W–OE2 = 2.93 ± 0.17		DA
GalO2–W–GLU129-OE2	OH–W = 2.85 ± 0.17		W–OE2 = 2.94 ± 0.16		AA
GalO2–W–GalNAc-N2	OH–W = 2.78 ± 0.15		W–O = 2.86 ± 0.12		DD
GalO3–W–ASP83-OD1	OH–W = 2.74 ± 0.14		W–OD1 = 2.74 ± 0.12		AA
GalO3–W–ASP83-OD2	OH–W = 2.90 ± 0.20		W–OD2 = 2.82 ± 0.14		AA
GalO3–W–SER126-O	OH–W = 2.67 ± 0.10		W–O = 2.90 ± 0.17		DA
GalO3–W–ASN127-ND2	OH–W = 2.72 ± 0.13		W–ND2 = 2.96 ± 0.16		DD
GalO3–W–GLU129-OE1	OH–W = 2.71 ± 0.13		W–OD1 = 2.88 ± 0.15		DA
GalO3–W–GLU129-OE2	OH–W = 2.74 ± 0.15		W–OE2 = 2.97 ± 0.16		DA
GalO6–W–ASP80-OD1	OH–W = 2.73 ± 0.16		W–OD1 = 2.89 ± 0.17		DA
GalO6–W–ASP80-OD2	OH–W = 2.82 ± 0.15		W–OD2 = 2.83 ± 0.12		AA
GalO6–W–ASP80-OD2	OH–W = 2.69 ± 0.14		W–OD2 = 2.83 ± 0.13		DA
GalO6–W–TYR125-OH	OH–W = 2.76 ± 0.12		W–OH = 2.88 ±0.18		AA
GalO6–W–GalNAcO6	OH–W = 2.80 ± 0.14		W–OH = 2.72 ± 0.12		AD
GalO6–W–GalNAcO6	OH–W = 2.79 ± 0.15		W–OH = 2.81 ± 0.16		AA
GalNAcO1–W–ILE101-O	OH–W = 2.82 ± 0.15		W–O = 2.73 ± 0.12		AA
GalNAcO1–W–ILE101-O	OH–W = 2.75 ± 0.13		W–O = 2.76 ± 0.13		DA
GalNAcO1–W–ASN41-ND2	OH–W = 2.85 ± 0.16		W–ND2 = 3.05 ± 0.16		AD
GalNAcO1–W–LEU212-N	OH–W = 2.92 ± 0.17		W–N = 2.99 ± 0.16		AD
GalNAcO1–W–GalNAcO4	OH–W = 2.94 ± 0.21		W–OH = 2.87 ± 0.21		DD
GalNAcO1–W–GalNAcO7	OH–W = 2.92 ± 0.17		W–OH = 2.71 ± 0.12		AA
GalNAcO4–W–ASN41-N	OH–W = 2.87 ± 0.16		W–N = 3.16 ± 0.14		DD
GalNAcO4–W–LEU212-N	OH–W = 2.76 ± 0.15		W–N = 3.01 ± 0.15		DD
GalNAcO4–W–GalNAcO7	OH–W = 2.83 ± 0.17		W–OH = 2.76 ± 0.17		DA
GalNAcO6–W–ASP80-OD1	OH–W = 2.68 ± 0.11		W–OD1 = 2.87 ± 0.15		DA
GalNAcO7–W–ASN41-ND2[a]	OH–W = 2.69 ± 0.14	2.81	W–ND2 = 3.06 ± 0.16	2.61	AD
GalNAcO7–W–ILE101-O[a]	OH–W = 2.66 ± 0.13	3.04	W–O = 2.77 ± 0.13	2.94	AA
GalNAcO7–W–LEU212-N[a]	OH–W = 2.73 ± 0.14	2.81	W–N = 3.02 ± 0.16	2.79	AD
GalNAcO7–W–GLY103-N	OH–W = 2.61 ± 0.09		W–N = 2.96 ± 0.14		AD
GalNAcO7–W–SER211-OG	OH–W = 2.62 ± 0.09		W–OG = 2.65 ± 0.10		AD

Experimental values correspond to the monomer.
[a] Crystallographic hydrogen bonds.

Table 5
T-antigen intramolecular water-mediated interactions

Hydrogen bond	In complex		Type	In solution	
	Mean lifetime (ps)	*P* (%)		Mean lifetime (ps)	*P* (%)
GalO1/GalNAcO3–W–GalNAcO7			AA	0.25	2
GalO2–W–GalNAc-N2			AD	0.42	9
	0.33	6	DD		
GalO3–W–GalO4			DD	0.48	4
GalO4–W–GalO6			DD	0.64	2
GalO5–W–GalNAcO7			AA	0.54	4
GalO5–W—GalNAcO4			AD	0.34	4
GalO6–W–GalNAcO4			AA	0.68	2
GalO6–W–GalNAcO6	0.69	24	AD		
	0.83	7	AA		
GalNAcO1–W–GalNAcO4	0.17	1	DD		
GalNAcO1–W–GalNAcO7	0.34	5	AA	0.34	2
GalNAcO4–W–GalNAcO7			AA	0.38	4
			AD	0.72	3
	0.53	7	DA		

P is expressed as percentage and represents the persistence of the hydrogen bond during the simulation time. Column ‘type’ indicates the donor or acceptor character: acceptor–acceptor (AA); donor–acceptor (DA); acceptor–donor (AD); donor–donor (DD). The first letter makes reference to the carbohydrate molecule first group.

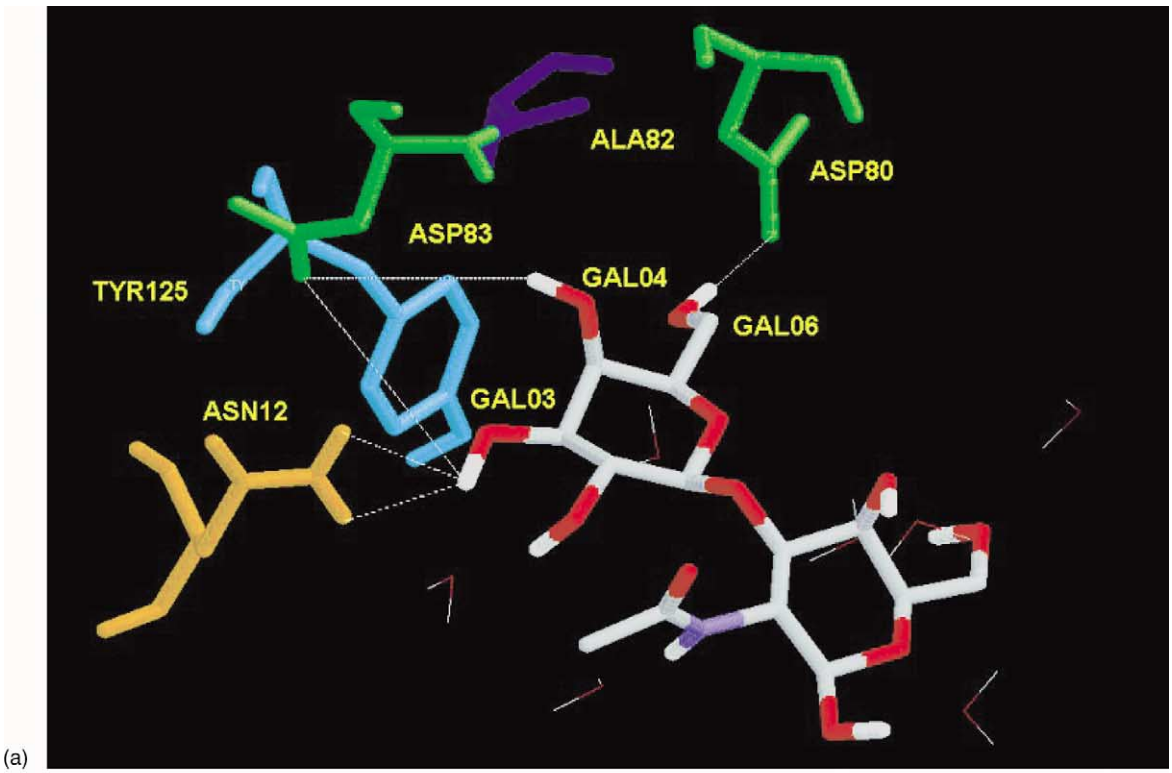

(a)

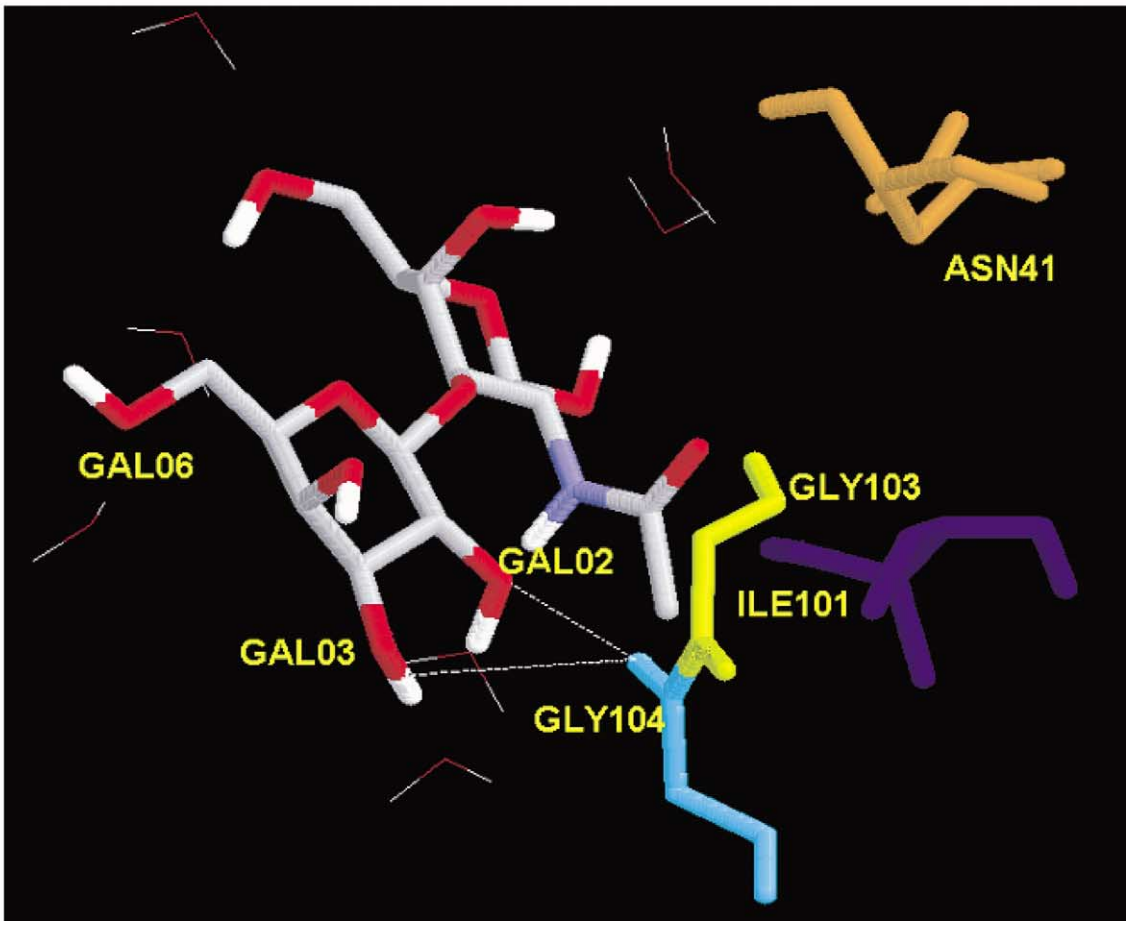

(b)

Fig. 3. (a–c) Snapshot of the configuration of a region of the active site. Several water molecules, some of them capable to form water bridges, are observed. Some possible hydrogen bonds are shown. Note that not all bonds shown are formed simultaneously, therefore this picture should not be considered as showing bifurcated hydrogen bond (plotted with RASMOL).

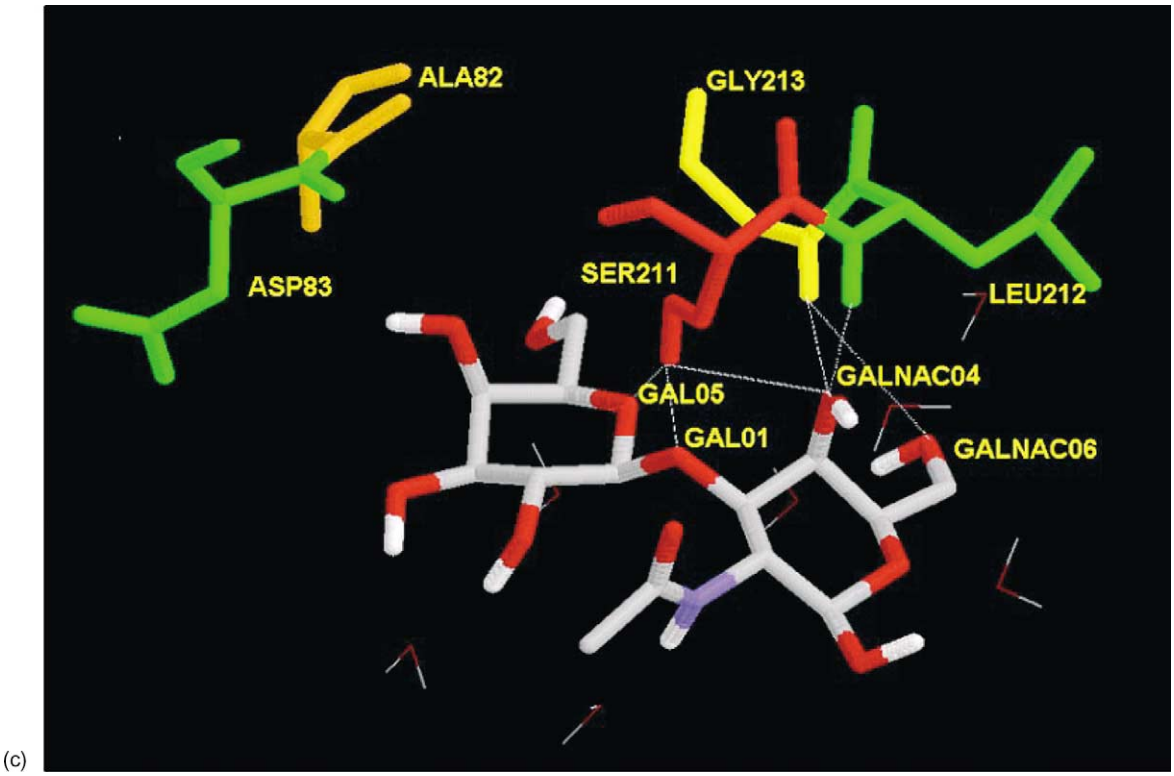

(c)

Fig. 3 (*Continued*).

long; rather they are in constant motion. To investigate the behavior of water molecules within the site in more detail, we monitored the trajectories of each and the formation of water bridges. We observed that there was a constant exchange of water molecules forming bridges mainly around GLU129, ASN127 and GLY104. Apparently five different water molecules were involved in forming the GalO2–W–GLU129 water bridge during the simulated 400 ps, and we counted up to eight different water molecules in the non-crystallographic water bridge GalO3–W–GLU129. The exchange was less frequent in water bridges established around LEU212, ASN41 and SER211, where we computed barely two different water molecules during the total simulated time.

3.5. T-antigen glyscosidic linkage dynamical evolution

The temporal evolution of the glycosidic angles was also monitored during the simulation process. Figs. 3 and 4 show the temporal evolution of the PHI (H–C1–O1–C3′) and PSI

Table 6
Water residence mean times calculated as the time that a water molecule remains in the sphere of radius 3.5 Å centred in the position of the T-antigen atoms capable of forming hydrogen bonds

Atom	In-complex water mean time (ps)	*Q* (%)	In-solution water mean time (ps)	*Q* (%)
GalO2	0.96	1	0.95	0
GalO3	1.00	25	0.96	0
GalO4	0.14	100	1.02	0
GalO5	0.17	70	0.71	3
GalO6	0.65	1	0.84	0
GalNAcO1	1.10	7	0.89	0
GalNAcN2	2.68	0.5	0.79	1
GalNAcO3	0.12	97	0.69	7.5
GalNAcO4	0.71	54	1.07	0
GalNAcO5	0.53	22	0.69	2
GalNAcO6	1.65	1	0.83	0
GalNAcO7	3.01	13	0.92	0

Q is defined as the ratio (expressed as a percentage) of the time that at least one water molecule was found within the sphere centred on a particular atom of the T-antigen and the total simulation time.

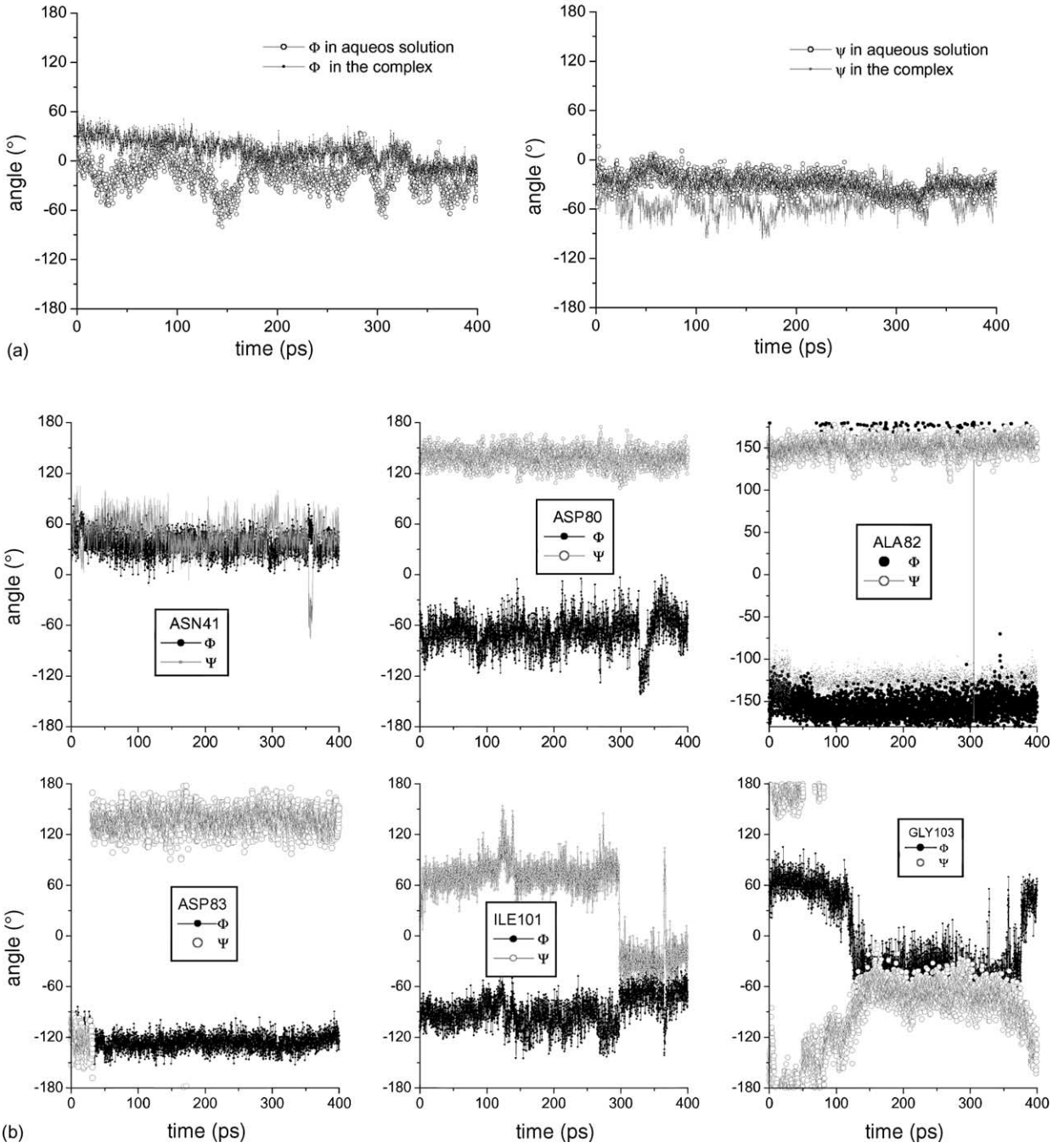

Fig. 4. (a) Temporal evolution of the torsion angles Φ (H–C1–O1–C3′) and ψ (H–C3′–O1–C1) of the glycosidic linkage. (b) Temporal evolution of the peptide bonds between amino acids situated less than 4.0 Å from any atom of the T-antigen.

(H–C3′–O1–C1) angles. Although it is necessary to perform simulations for longer than 400 ps to observe large conformational changes of the T-antigen linkage [16], we were able to see marked differences between the free and complexed states. Mean values for the PHI and PSI angles differed when the molecule was in solution and when it is in the active site. The PSI angle was less mobile than the PHI angle in solution, and the situation was reversed in complex. As expected, PHI and PSI angles behaved more rigidly in complex because the T-antigen is anchored by hydrogen bonds and water-mediated interactions between the protein and the sugar rings. Although the molecule in solution is very flexible, we were able to estimate the mean values of the PHI and PSI angles to be -17 ± 18 and $-52 \pm 14^{\circ}$, respectively. These values changed when the torsion angles were measured in complex; the new conformation was measured to be $25^{\circ} \pm 12^{\circ}$ and $-20^{\circ} \pm 17^{\circ}$ for the PHI and PSI angles, respectively, which is in good agreement with

the torsion values obtained using the crystallographic data (PHI = 21°, PSI = −16°).

During the simulation, the disaccharide did not undergo significant conformational changes. None of the sugar rings changed their chair conformations during either the in-solution or in-complex simulations. We also monitored the behavior of the peptide bond dihedral angles of the amino acids that were less than 4.0 Å from any atom of the T-antigen to see whether any of them exhibited important structural changes, and in each case we observed a large dispersion indicative of the high mobility of the active site.

With the exception of GLY104 and ASN127, none of the amino acids involved in the formation of direct hydrogen bonds (ASP83, ASP80, SER211 and GLY213) exhibited important torsional changes. The adjacent residues (GLY103 and GLY104) were very mobile, and the conformational changes they exhibited occurred at approximately the same time. Monitoring the water bridges established by these two amino acids, we observed that their formation was favored when the dihedral angles were about −100 or 35.5° during the first 100 ps and at the end of the simulation. Because ILE101 was more exposed to the water environment, it had a greater probability of transition. In that regard, the new conformation allowed the entrance of water molecules into the site, thus making possible the formation of water bridges.

3.6. Mean number of water molecules in the active site and temporal evolution of the T-antigen center of mass

Another important point to be considered is T-antigen hydration. When we calculated the number of water molecules within a 3.5 Å radius of any atom of the molecule, we obtained a mean of 13.4 ± 2.6 water molecules for complexed T-antigen, indicating that it remains well hydrated most of the time. The hydration number of the T-antigen in solution was 32.9 ± 4.1. This means that a total of almost three water molecules per atom are capable of forming hydrogen bonds, and that this number is reduced to one water molecule per atom when the antigen is in complex.

The trajectory of the T-antigen center of mass was calculated taking the center of the sphere as the origin. The T-antigen remained very stable in complex, anchored by direct and water-mediated interactions at all times. The mean value of the dispersion was 1.21 Å with a standard deviation of 0.224 Å.

4. Conclusions

The stochastic dynamics simulations described here reproduced the main structural and dynamical characteristics of the PNA lectin active site interacting with T-antigen disaccharide. The molecular structure of the spherical region was maintained not only by the mean boundary forces, but also by the contribution of forces computed using of the previously calculated electrostatic potential values at lattice points. Our goal was to apply this methodology, developed by Oberlin and Scheraga [26], to carry out a more realistic simulation, and the results obtained are in good agreement with the crystallographic findings.

As crystallographic analysis previously showed [5], the T-antigen is held in the active site by means of a strong network of direct and water-mediated interactions. In addition to those demonstrated by X-ray crystallography, we observed other frequently occurring and long lasting direct interactions, especially between GalNAcO7 and various amino acids at the site. The direct interactions between this particular atom and the PNA lectin may reflect the slightly different location of the T-antigen within the binding site predicted by our simulation and that found in the crystallographic data. The number of water-mediated interactions between the PNA lectin and the T-antigen observed during the simulations is larger than in the crystal due to the large number of water molecules that have access to the site. Their small volume and their high mobility allow them to generate water bridges between the sugar and different atoms of the same amino acid, which may help to strengthen the intermolecular interaction.

Either the small difference in the interaction of the GalNAcO7 and the different number of water in the active site, comparing with the diffraction experiment should not be a surprise. Water, as well as mobile parts on solutes, is difficult to observe by X-rays diffraction due to its experimental time scale. Mobile water molecules, and even side chains or ending of small molecules can blur the signal producing noise. On the other hand, the inclusion of water in the regular crystallographic procedure induce to believe that all water are frozen in fixed position. We must bear in mind that the number and the dynamical state of water are strongly dependent of the model [28]. One of the main contributions of the dynamics simulation is to complement the static view of crystallography, approaching more to the ‘in vivo’ state.

The intra-saccharide, water-mediated interaction between the GalO6 and GalNAcO6 occurs very frequently and might have a role in helping to maintain the extended conformation of the saccharide. One aspect that can be analyzed using MD is the hydration number of the interacting site. We could see that the binding site keeps itself hydrated; there was a mean of 13 water molecules within a 3.5 Å radius from any atom of the T-antigen. We also noted that there is apparently a constant exchange of water molecules with the bulk, as was evidenced by the short mean residence times and by the trajectories of water molecules during the formation of water bridges. The exchange of water molecules with bulk happens mainly in the proximity of GLU129, ASN127 and GLY104. This constant motion of water molecules within the active site may influence the conformational transitions of amino acids closer to the T-antigen molecule, with some preferred conformations being related to the formation of water bridges.

In sum, we have used MD simulation to reveal hydration sites, residence times of water molecules around the substrate, and the mean lifetime and relative frequency of persistence of hydrogen bond formation between PNA lectin and T-antigen in complex. These data are a complement of the existing crystallographic information.

Acknowledgements

FAPERJ and CABBIO resources supported this work. We also want to thank to the PRONEX program CONICET and ANPCyT. JRG is member of the Carrera del Investigador of CONICET.

References

[1] W.J. Peumans, E.J.M. van Damme, Lectins as plant defense proteins, Plant Physiol. 109 (1995) 347.
[2] K. Suguna, A. Surolia, M. Vijayan, Structural Diversity and Carbohydrate Specificity of Plant Lectins. Perspectives in Structural Biology, Universities Press (India) Ltd., 1999, pp. 367–379.
[3] G.N. Reeke Jr., J.W. Becker, Carbohydrate-binding sites of plant lectins, Curr. Topics Microbiol. Immunol. 120 (1985) 35–58.
[4] R. Baneerj, S. Mande, V. Ganesh, K. Das, V. Dhanarj, S. Mantha, K. Suguna, A. Surolia, M. Vijayan, Crystal structure of peanut lectin, a protein with a unusual quaternary structure, Proc. Natl. Acad. Sci. U.S.A. 91 (1994) 227–231.
[5] J.E. Toone, Structure and energetics of protein–carbohydrate complexes, Curr. Opin. Struc. Biol. 4 (1994) 719–728.
[6] R. Loris, F. Casset, J. Bouckaert, J. Pletinckx, M. Dao-Thi, F. Poortmans, A. Imberty, S. Perez, L. Wyns, The monosaccharide binding site of lectil lectin: an X-ray and molecular modelling study, Glycoconjugate J. 11 (1994) 507–517.
[7] R. Baneerj, K. Das, R. Ravishankar, K. Suguna, A. Surolia, M. Vijayan, Conformation, protein carbohydrate interactions and a novel subunit association in the refined structure of peanut lectin–lactose complex, J. Mol. Biol. 259 (1996) 281–296.
[8] R. Ravishankar, K. Suguna, A. Surolia, M. Vijayan, Crystal structure of the peanut–T-antigen complex. Carbohydrate specificity generated by water bridges, Curr. Sci. 72 (11) (1997) 855–861.
[9] H.M. Berman, J. Westbrook, Z. Feng, G. Gilliland, T.N. Bhat, H. Weissig, I.N. Shindyalov, P.E. Bourne, The Protein Data Bank, Nucleic Acids Res. 28 (2000) 235–242.
[10] G. Springer, T and tn, general carcinoma auto-antigens, Science 224 (1984) 1198–1206.
[11] T. Irimura, T. Kawaguchi, T. Terao, T. Osawa, Carbohydrate-binding specificity of so-called galactose-specific phytohemagglutinins, Carbohydr. Res. 39 (1975) 317–327.
[12] R. Lotan, E. Skutelsky, D. Danon, N. Sharon, Purification, composition, and specificity of anti-T lectin from peanut (arachis-hypogaea), J. Biol. Chem. 250 (1975) 8518–8523.
[13] X. Lee, A. Thompson, Z. Zhang, H. Ton-that, J. Biesterfeldt, C. Ogata, L. Xu, R. Jhonston, M. Young, Structure of the complex of Maclura Pomifera agglutinin and the T-antigen disaccharide, Galβ(1–3)GalNAc, J. Biol. Chem. 273 (11) (1998) 6312–6318.
[14] G.M. Bradbrook, T. Gleichmann, S.J. Harrop, J. Habash, J. Raftery, J. Kalb(Gilboa), J. Yariv, I.H. Hilier, J.R. Helliwell, X-ray and molecular dynamics studies of concanavalin–A glucoside and mannoside complexes. Relating structure to thermodynamics, Faraday Trans. 94 (1998) 1603–1611.
[15] R. Loris, P.P.G. Stas, L.J. Wyns, Conserved waters in legume lectin crystal structures, J. Biol. Chem. 269 (43) (1994) 26722–26733.
[16] K.J. Naidoo, J.W. Brady, Molecular dynamics simulations of a glycoprotein: the lectin from *Erythrina corallodendron*, J. Mol. Struc. (Theochem.) 395–396 (1997) 469–475.
[17] G.M. Bradbrook, J.R. Forshaw, S. Pérez, Structure/thermodynamics relationships of lectin saccharide complexes. The *Erythrina corallodendron* case, Eur. J. Biochem 267 (2000) 4545–4555.
[18] J. Åqvist, S.L. Mowbray, Sugar recognition by a glucose/galactose receptor, J. Biol. Chem. 270 (17) (1995) 9978–9981.
[19] P. Pascutti, L. El-Jaik, P. Bisch, K. Mundim, A. Ito, Molecular dynamics simulation of α-melanocyte stimulating hormone in a water–membrane model interface, Eur. Biophys. J. 28 (6) (1999) 499–509.
[20] W.F. Van Gunsteren, H.J.C. Berendsen, GROMOS from BIOMOS, n.v, Nijenborg 4, 9747, AG Groningen, 1987.
[21] W.F. Van Gunsteren, S. Billeter, A. Eising, P. Hünenberger, P. Krüger, A. Mark, W. Scott, I. Tironi, Biomolecular Simulation: The Gromos96 Manual and User guide, vdf Hochschulverlag AG na der ETH Zürich and BIOMOS b.v., Zürich, Groningen, 1996.
[22] H.J.C. Berendsen, J.R. Grigera, T.P. Straatsma, The missing term in the effective pair potentials, J. Phys. Chem. 91 (1987) 6269–6271.
[23] C.L. Brooks, M. Karplus, Solvent effect on protein motion and protein effects on solvent motions. Dynamics of the active site region of lisozyme, J. Mol. Biol. 208 (1989) 159–181.
[24] W.F. Van Gunsteren, H.J.C. Berendsen, A leap frog algorithm for stochastic dynamics, Mol. Simul. 1 (1988) 173–185.
[25] C. Post, B. Brooks, M. Karplus, C. Dobson, P. Artymiuk, J. Cheetham, D. Phillips, Molecular dynamics simulations of native and substrate-bound lysozyme, J. Mol. Biol. 190 (1986) 455–479.
[26] D. Oberlin, H.A. Scheraga, B-spline method for energy minimization in grid-based molecular mechanics calculations, J. Comp. Chem. 19 (1) (1998) 71–85.
[27] E.R. Caffarena, P.M. Bisch, Hydration of T-antigen Galβ(1–3)GalNAc and the isomer Galβ(1–3)GlcNAc by molecular dynamics simulations, J. Mol. Graph. Mod. 18 (2000) 119–125.
[28] A.D. Podjarny, E.I. Howard, A. Urzhumtsev, J.R. Grigera, A multicopy modelling of the water distribution in macromolecular crystals, Proteins: Struc. Function Genet. 28 (1997) 303–312.